Stagnant dip layer-by-layer assembly

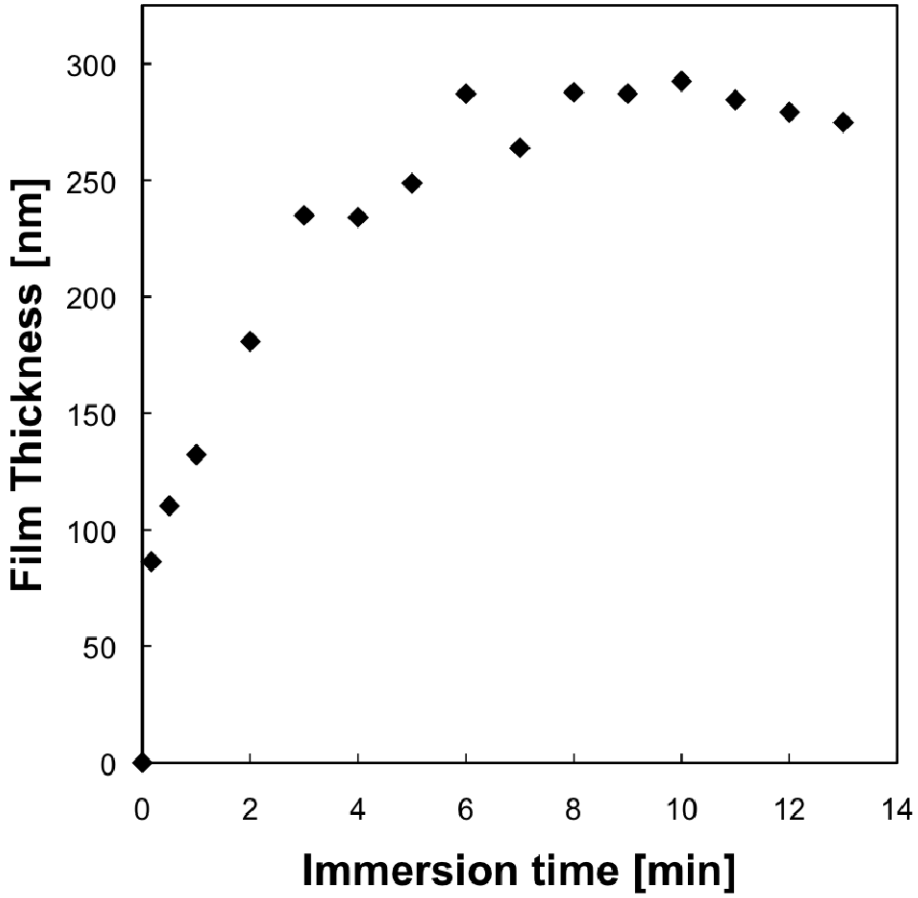

Figure S1. Dip layer-by-layer assembly of oppositely charged nanoparticles in stagnant solution. Nanoparticle suspensions are 0.38 mg/mL positively charged SiO_2 and 0.38 mg/mL negatively charged SiO_2 and substrates are microscope glass slides. The dip LbL procedure is: immersion in positively charged SiO_2 nanoparticle solution for a specified duration, sequential immersion in three deionized water rinse baths for 2 minutes, 1 minute, 1 minute, respectively, immersion in negatively charged SiO_2 nanoparticle solution for the same amount of time as the positive SiO_2 bath, and finally immersion in another three deionized water rinse baths for 2 minutes, 1 minute, 1 minute, respectively. The entire cycle is carried out 10 times. The standard deviation in each data point is less than 10 nm based on the measurement of at least two samples prepared simultaneously.

Demonstration of fast cationic particle adsorption

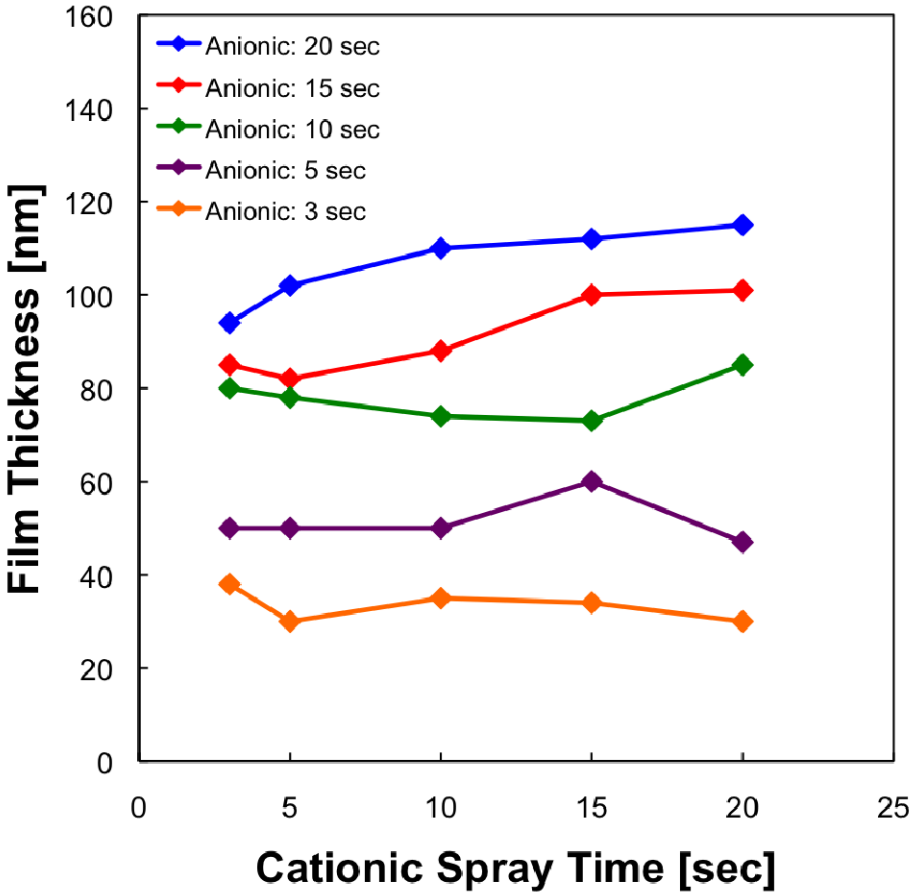

Figure S2. Thickness of spray LbL nanoparticle films as a function of spray time per cationic deposition step for constant anionic spray times. Films were prepared according to the techniques described in the Experimental Methods section, using 0.38 mg/mL cationic suspensions and 6.5 mL/s spray flow rates in 5 complete deposition cycles (5 cationic steps and 5 anionic steps). The spray time for anionic solution per deposition step is represented by data series color: 20 sec (blue), 15 sec (red), 10 sec (green), 5 sec (purple), 3 sec (orange). The spray time for cationic solution per deposition step is reported on the x-axis. The data indicate that film thickness is nearly independent of cationic solution spray time for any given anionic solution spray time within the range of times studied. Therefore, cationic nanoparticles (12 nm diameter) achieve saturation of the available adsorption surface extremely quickly relative to the time scales considered. Deposition of anionic nanoparticles (22 nm diameter) is much slower, and film thickness is observed to be a strong function of anionic spray time. The standard deviation in each data point is less than 5 nm based on at least three measurements made on each sample.

Demonstration of linear film growth with bilayer number

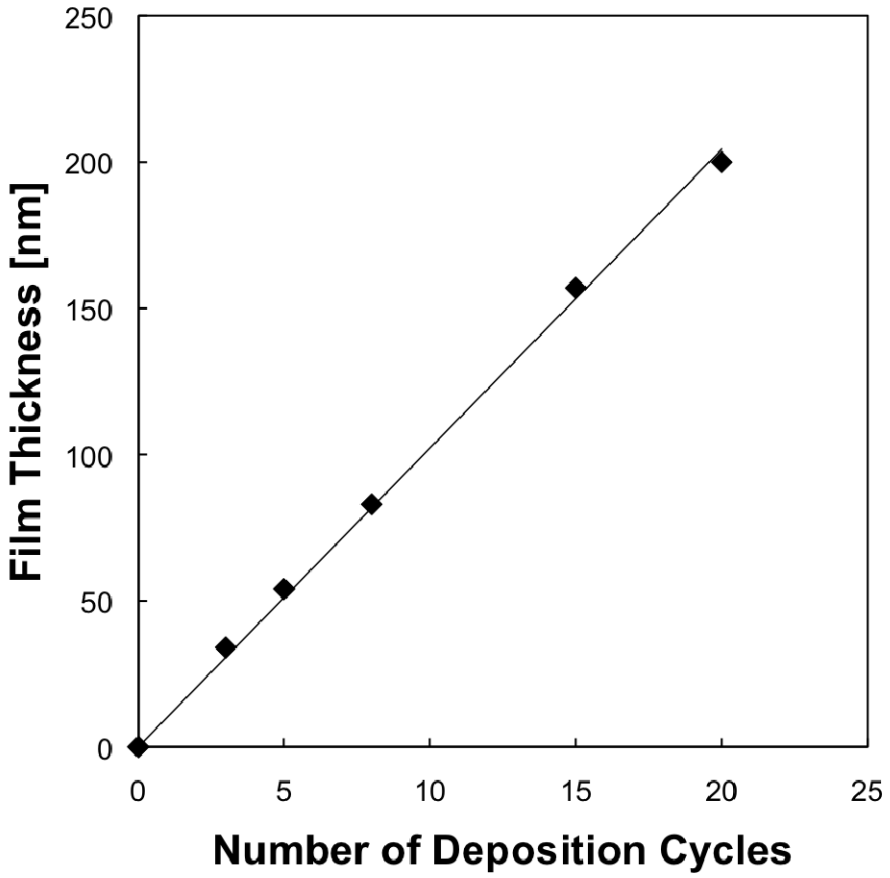

Figure S3. Thickness of spray LbL nanoparticle films as a function of the number of deposition cycles. Films were prepared according to the techniques described in the Experimental Methods section, using identical operating parameters for each deposition cycle: 0.38 mg/mL cationic and anionic suspensions, 0.8 mL/s spray flow rates, and 10 second spray times per deposition step. Film growth as a function of the number of deposition cycles can be fitted to a straight line with an R^2 value of 0.997. Note that deposition thickness increases linearly with the number of cycles even though nanoparticle saturation was not reached during any step. The standard deviation in each data point is less than 5 nm based on at least three measurements made on each sample.

Derivation of the kinetic model for multilayer films

The deposition kinetics of individual nanoparticle layers composed of a single species can be simply and accurately described using a first-order model. However, for the purposes of our study we must develop a model for the overall deposition kinetics of a multilayer film. We begin with the adsorption model for each constituent deposition step:

$$m_i = m_{\max,i}\left[1-\exp\left(-\alpha_i t\right)\right]. \qquad \text{(S-1)}$$

Here, the subscript i refers to the corresponding deposition step (i = 1, 2, …, 20) and we note that the maximum adsorbed nanoparticle mass per deposition stage, m_{max}, and the characteristic deposition rate constant, α, can vary between steps. The exact, full form of the equation for the total nanoparticle mass adsorbed after 20 deposition steps, M, is then:

$$M = m_1 + m_2 + \ldots + m_{20} \qquad \text{(S-2a)}$$

or

$$M = m_{\max,1}\left[1-\exp\left(-\alpha_1 t\right)\right] + m_{\max,2}\left[1-\exp\left(-\alpha_2 t\right)\right] + \ldots + m_{\max,20}\left[1-\exp\left(-\alpha_{20} t\right)\right] \quad . \qquad \text{(S-2b)}$$

Odd-indexed terms in the sum refer to cationic deposition steps and even-indexed terms refer to anionic deposition steps. In our experiment, each deposition stage is applied for the same duration t.

Equation S-2b contains 40 unknown parameters and is prohibitively difficult to work with. We can simplify the equation considerably with minimal loss of predictive accuracy by applying the experimental findings of Figure S-2, Figure S-3, and knowledge of the transport limitations of nanoparticle LbL deposition. First, Figure S-2 implies that the deposition of our cationic silica nanoparticles (nominal diameter 12 nm) occurs extremely rapidly relative to the time scales of our experiment. The disparity in deposition rate between cationic and anionic particles may arise from the different hydrodynamic properties of particles with different sizes. We anticipate that the smaller nanoparticles have a higher diffusivity through the aqueous medium, which likely accelerates the mass transport process associated with deposition. In fact, we can reasonably approximate that cationic nanoparticles completely saturate the entire available adsorption surface for all deposition times studied in this experiment. So, for all cationic deposition stages we can assume that the cationic deposition rate constant is very large and $\alpha_{cation,\,i} \cdot t >> 1$. Therefore $m_i \approx m_{max,\,i}$ for all odd i.

Second, it has been demonstrated that the LbL deposition of silica nanoparticles is kinetically controlled by the mass transport rate of nanoparticles towards the substrate.[1] The mass transport process is identical for each deposition stage using the same type of nanoparticle, since we maintain identical LbL operating parameters between deposition steps. That is, the two mass transport zones in Figure 1 of the main paper remain identical during each cationic step or each anionic step. The fluid mechanical properties of our large anionic particles may differ from those of our small cationic particles, so we cannot claim that all 20 deposition stages have identical transport kinetics. However, all 10 anionic deposition stages do share identical transport kinetics.

The assumption of identical deposition kinetics across all deposition cycles is supported by the linear relationship between film thickness and number of deposition cycles, as shown in Figure #-3. Therefore $\alpha_2 = \alpha_4 = \ldots = \alpha_{20}$. If we let α_{anion} be the characteristic rate constant for anionic deposition steps, then $\alpha_i = \alpha_{anion}$ for all even i.

Finally, we assume that the saturation mass of each deposition step, m_{max}, is proportional to the surface coverage of the opposite material (or the uncovered substrate, for cationic particles) at the start of the deposition step. We believe that this assumption is justified as the LbL process relies on electrostatic interactions of oppositely charged species, so the exposed area of the opposite material defines the potential surface available for adsorption. Since nanoparticles deposit as single-particle-depth layers, the exposed surface area resulting from a deposition stage is proportional to deposited mass. The proportionality constant may be different for cationic and anionic material, but it should be the same across subsequent depositions of the same material. Again, the assumption of similar kinetics across subsequent deposition cycles is supported by the data in Figure S-3.

The potential surface for adsorption during the first cationic deposition stage is the entire bare substrate. Based on the approximation that our small cationic nanoparticles achieve saturation very quickly, we assume that the substrate surface always becomes saturated during deposition stage 1. Since all experiments use identically sized glass substrates, the adsorption mass during stage 1 is simply a constant, A:

$$m_1 = A \,. \qquad \text{(S-3)}$$

The saturation mass of anionic particles during the second deposition step is then proportional to the constant deposition mass during the first cationic step. Defining *a* as the proportionality constant for anionic deposition onto cationic material, we have:

$$m_{\max,2} = aA \qquad \text{(S-4a)}$$

or

$$m_2 = aA\left[1 - \exp\left(-\alpha_{anion} t\right)\right] . \qquad \text{(S-4b)}$$

The saturation mass of cationic nanoparticles in the third deposition step is proportional to the total deposited mass of TM in the previous step. All of the binding sites for the cationic particles have been taken up in step 1, so there is no exposed substrate surface for adsorption and the only available adsorption surface is defined by the previous anionic deposition. Defining *b* as the proportionality constant for cationic deposition onto anionic material, and noting that $m_i \approx m_{max,\,i}$ for cationic steps, we have:

$$m_3 = m_{\max,3} = bm_2 \qquad \text{(S-5a)}$$

or

$$m_3 = baA\left[1 - \exp\left(-\alpha_{anion} t\right)\right] . \qquad \text{(S-5b)}$$

Now, recall that cationic material accomplishes saturation of the available surface quickly relative to our experiment's time scales. This means that at the start of each anionic step the entire substrate surface is saturated with cationic particles, having completely coated all anionic surface coverage from the previous step. In other words, the exposed mass of cationic particles acting as potential adsorption sites for anionic particles is always equal to A (the mass of cationic particles associated with total substrate surface coverage). Using the same proportionality relationship between maximum anionic adsorption mass and current exposed cationic mass, we have:

$$m_{\max,4} = aA \quad . \tag{S-6a}$$

In fact:

$$m_{\max,i} = aA \qquad \text{for all even } i. \tag{S-6b}$$

$$mi = aA\left[1-\exp\left(-\alpha_{anion}t\right)\right] \qquad \text{for all even } i. \tag{S-6c}$$

By applying the same logic of cationic deposition that led to Equation S-5b, we have:

$$m_i = baA\left[1-\exp\left(-\alpha_{anion}t\right)\right] \qquad \text{for all odd } i \text{ excluding } i = 1. \tag{S-7}$$

Substitution into Equation S-2a gives:

$$M = A + aA\left[1-\exp\left(-\alpha_{anion}t\right)\right] + baA\left[1-\exp\left(-\alpha_{anion}t\right)\right] + aA\left[1-\exp\left(-\alpha_{anion}t\right)\right] + \ldots \qquad \text{(S-8a)}$$

which can be reduced by combining terms to:

$$M = A + \left(10aA + 9baA\right)\left[1-\exp\left(-\alpha_{anion}t\right)\right] \quad . \qquad \text{(S-8b)}$$

We observe that (10 a A + 9 b a A) is a constant, which we can call B:

$$M = A + B\left[1-\exp\left(-\alpha_{anion}t\right)\right] \quad . \qquad \text{(S-8c)}$$

To complete the derivation, we note that the constant A refers to the mass of nanoparticles in the first deposition layer, while B (1 – exp[-α_{anion} t]) refers to the mass of nanoparticles in the subsequent 19 layers. As long as deposition time is not extremely small, the mass of the first deposition layer will be much less than the mass of the following 19 layers. We therefore incur little error by neglecting the constant A term. We rename the pre-factor of the exponential term M_{max}, as it now corresponds to the maximum saturation mass of nanoparticles in the multilayer film as time approaches infinity:

$$M = M_{\max}\left[1-\exp\left(-\alpha_{anion}t\right)\right] \quad . \qquad \text{(S-9)}$$

Statistical p-values on spray LbL operating parameters

To study the effect of each processing parameter in detail, we perform statistical analysis on film thickness as a function of each individual operating parameter (refer to Figure 2 for the raw data). Analysis confirms a strong positive correlation between film thickness and each operating parameter. We find correlation p-values of $p = 0.000$ for concentration, $p = 0.023$ for flow rate, and $p = 0.000$ for spray time using a standard 0.05 significance level. Each calculated p-value is much smaller than the significance level. Thus we are confident that the observed correlations between operating parameters and film thickness are statistically significant and not due to random sampling variations.

We use the Minitab statistical software package to generate p-values for our data sets. A p-value is defined as the probability that an observed test statistic, or a more extreme test statistic, could be obtained assuming that some null hypothesis is true.[2] In our case, the test statistic is the strength of the correlation between an operating condition and film thickness (an extreme test statistic is a very strong correlation). Our hypothesis is that the operating condition indeed affects film thickness, and that the correlation is not coincidence. The null hypothesis, then, states that any observed effects are coincidental. We seek a mathematical justification to reject the null hypothesis. We supply two data sets to the computer software package (for example, a list of suspension concentrations and the corresponding film thicknesses), which returns a p-value for the probability that any observed correlation between the two data sets could have occurred by chance alone. If this p-value is lower than a standard value of 0.05, we confirm that the null hypothesis is likely false and the correlation is statistically significant.

Notes and References

1. Y. M. Lvov, J. F. Rusling, D. L. Thomsen, F. Papadimitrakopoulos, T. Kawakami and T. Kunitake, *Chemical Communications*, 1998, 1229-1230.

2. N. A. Weiss, *Introductory Statistics*, Addison-Wesley, 2011.